Selective Modal Transducers for Anisotropic Rectangular Plates: Experimental Validation

Scott E. Miller[*]

Hughes Space and Communications Company, El Segundo, California 90245

and

Haim Abramovich[†] and Yaakov Oshman[†]

Technion—Israel Institute of Technology, Haifa 32000, Israel

A general selective modal transducer (SMT) design methodology recently introduced by the authors for piezo-laminated anisotropic plate systems is validated through an experimental test on a cantilevered orthotropic composite piezolaminated plate. Fundamental aspects of the SMT theory are reviewed. The SMT theory is extended to provide the means to predict the modal character of multilayered piezolaminated transducers embedded in an anisotropic plate in which the active subelements are both bidirectional and spatially varying. An experimental procedure is described involving a 10-layered orthotropic plate constructed from four graphite-epoxy layers sandwiched between six piezoelectrically active polyvinylidine fluoride (PVDF) sublaminae. Three PVDF sublaminae stacked on one face are combined electrically to provide a single sensed measurement, while the three remaining PVDF sublaminae stacked on the opposing face are combined to provide single channel actuation. Lead compensation is employed to provide active control. Open- and closed-loop frequency and transient response data are then analyzed, and significant active vibration attenuation is observed. A numerical simulation directly based on an SMT-derived transducer model is developed, and simulation results are compared with observed system behavior. The theoretically based results closely resemble the measured response to within an expected range of accuracy, thus validating the transducer theoretical model predicted by the SMT theory.

I. Introduction

WITHIN the past decade, several vibration control techniques have been developed for simple beam and plate systems that utilize distributed piezoelectric transducers formed from polyvinylidine fluoride (PVDF). PVDF actuators have been designed whose spatially varying piezoelectric field properties were exploited to provide for the simultaneous control of all modes or special modal subsets in cantilevered and simply supported beams.[1,2] Miller and Hubbard[3] developed a reciprocal sensor theory and subsequently incorporated PVDF sensors and actuators into multicomponent systems in which each component itself was a smart structural member. Burke and Hubbard[4] developed a formulation for the control of thin elastic (Kirchhoff–Love) isotropic plates subject to most combinations of free, clamped, or pinned boundary conditions, in which the active elements were spatially varying biaxially polarized piezoelectric transducer layers. Lee[5] generalized the classical laminate plate theory to include the effect of laminated piezoelectric layers and thus to provide a theoretical framework for the distributed transduction of bending, torsion, shearing, shrinking, and stretching in flexible anisotropic plates. Miller et al.[6] subsequently employed Lyapunov's second method to derive a general active vibration suppression control design methodology for anisotropic laminated piezoelectric plates.

The aforementioned vibration control strategies share several common limitations. Perhaps most significantly, although all of these methods reduce the vibration control task to a selection of individual piezolaminae field functions, none offers a general method for determining those field functions so as to ensure active vibration suppression. Therefore a clearly defined design methodology was developed by the authors[7,8] in which the structural and control design processes are integrated to yield a framework for truly selective modal control (SMC). The SMC approach requires the implementation of selective modal transducers (SMTs) that utilize multiple piezolaminae to provide modal transduction based on a selected choice of modal participation factors (MPFs). A broad class of stability robust SMC approaches was defined through the identification of conditions that sufficiently ensure global asymptotic stability without requiring perfect knowledge of design parameters, structural constants, or modal behavior. Specific SMC design examples have been presented that allow for 1) the contributions of any given mode to the active energy extraction rate to be directly specified, 2) pole locations to be selectively and dynamically varied, or else 3) pole locations, SMT design parameters, and feedback laws to be optimally determined.

The SMC approach is contingent on the successful development of SMTs via proper implementation of the SMT theory. Although several numerical examples have been presented[7] that support both the SMT and SMC theories, the present study is primarily concerned with demonstrating the SMT concept on actual hardware. A secondary objective is to describe a means through which the SMT theory may be used in the converse sense to predict the MPFs associated with a given multilayered transducer and known piezospatial variance properties. To achieve these goals, a 10-layered skew symmetric orthotropic plate was constructed, consisting of four graphite-epoxy layers embedded between two SMTs. Each SMT contains three PVDF piezosublaminae and assumes either a pure sensing or pure actuation function. A simple lead compensation circuit that emulates a stability robust control law developed in Ref. 7 at low frequencies was constructed. The structure was cantilevered and excited externally through an electromagnetic coil. Open- and closed-loop frequency and transient response data were obtained for the first four structural modes. Using the SMT theory, the actual system behavior was predicted through numerical simulation. A comparison was then made between actual and predicted dynamic behavior, which effectively validates the SMC theory.

II. System Description

Figure 1 describes the geometry of the general system under consideration. A rectangular anisotropic plate with exactly N piezoelectrically active laminated layers is considered. Contrary to what may be implicitly assumed from Fig. 1, transducer layers may be located anywhere in the structure. The length dimensions of the system in
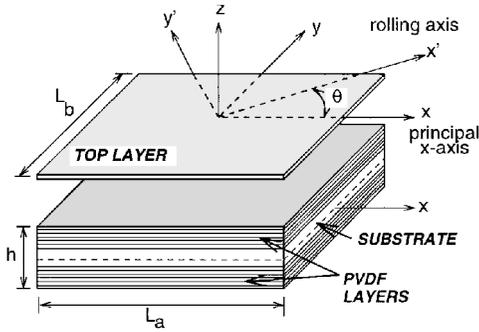
Fig. 1   General piezolaminated plate geometry.

the x and y directions are denoted as L_a and L_b, respectively. Each piezoelectric layer may be independently anisotropic, and its electromechanical field strength may be selectively varied in both spatial dimensions. The material properties within each lamina are assumed continuous. A complete system description may be found in Ref. 8.

Applying the well-known Kirchhoff–Love approximation, the authors developed the equations of motion of the general system described in Fig. 1 in Ref. 8, and the equations are expressed in the form

$$x_{tt} + Cx_t + \mathcal{K}x = -\frac{1}{\rho h}\mathcal{D}^T\left(\sum_{k=1}^{N} e_0^k \Lambda^k V^k\right) \tag{1}$$

where a subscript t indicates partial temporal differentiation,

$$\mathcal{D},\ \mathcal{E} \triangleq \begin{bmatrix} \frac{\partial}{\partial x} & \frac{\partial}{\partial y} & 0 & 0 & 0 & 0 \\[6pt] 0 & \frac{\partial}{\partial x} & \frac{\partial}{\partial y} & 0 & 0 & 0 \\[6pt] 0 & 0 & 0 & \frac{\partial^2}{\partial x^2} & 2\frac{\partial^2}{\partial x \partial y} & \frac{\partial^2}{\partial y^2} \end{bmatrix}^T$$

$$\begin{bmatrix} -\frac{\partial}{\partial x} & -\frac{\partial}{\partial y} & 0 & 0 & 0 & 0 \\[6pt] 0 & -\frac{\partial}{\partial x} & -\frac{\partial}{\partial y} & 0 & 0 & 0 \\[6pt] 0 & 0 & 0 & \frac{\partial^2}{\partial x^2} & 2\frac{\partial^2}{\partial x \partial y} & \frac{\partial^2}{\partial y^2} \end{bmatrix}^T \tag{2}$$

and

$$x \triangleq [u(x,y)\quad v(x,y)\quad w(x,y)]^T$$
$$\mathcal{K} \triangleq (1/\rho h)\mathcal{D}^T K_a \mathcal{E}, \qquad C \triangleq b_0 I + c_0 \mathcal{K} \tag{3}$$

The term $K_a \in \mathfrak{R}^{6,6}$ is the standard material stiffness matrix containing the usual A_{ij}, B_{ij}, and D_{ij} constitutive constants that characterize the mechanical stress–strain behavior of the composite system[8]; and u, v, and w are, respectively, the x, y, and z directional displacements. The constants b_0 and c_0 are viscous and structural damping coefficients, respectively, whereas I is the identity operator. The term $V^k = V^k(t)$ is the spatially independent driving voltage applied across the kth piezolamina. The electromechanical field strength of each piezolamina is described mathemetically via the product $e_0^k \Lambda^k$, where Λ^k is a dimensionless and spatially varying piezoelectric field distribution function (PFF). The vector e_0^k is defined as $e_0^k \triangleq [e_\star^k;\ z^k e_\star^k]$, where $e_\star^k \in \mathfrak{R}^3$ is a vector of piezoconstants relative to the point of maximum electromechanical transduction.

The boundary conditions as derived in Ref. 8 are stated in Table 1, where the in-plane resultant forces ($N \triangleq [N_1\ N_6\ N_2]^T$) and moments ($M \triangleq [M_1\ M_6\ M_2]^T$) are given by

$$\begin{bmatrix} N \\ M \end{bmatrix} = -K_a \mathcal{E}x - \sum_{k=1}^{N} e_0^k \Lambda^k V^k \tag{4}$$

Table 1   Boundary conditions

$x = -(L_a/2),\ (L_a/2)$	$y = -(L_b/2),\ (L_b/2)$
(N_1) or u	(N_2) or v
(N_6) or v	(N_6) or u
(Q_1) or w	(Q_2) or w
(M_1) or $\partial w/\partial x$	(M_2) or $\partial w/\partial y$
(M_6) or $\partial w/\partial y$	(M_6) or $\partial w/\partial x$

and the transverse shear force resultants Q_1 and Q_2 are defined as

$$Q_1 \triangleq \frac{\partial M_1}{\partial x} + \frac{\partial M_6}{\partial y}, \qquad Q_2 \triangleq \frac{\partial M_6}{\partial x} + \frac{\partial M_2}{\partial y} \tag{5}$$

Finally, the current flow and measured voltage across the kth lamina due to the mechanical displacement of the laminates were determined in Ref. 8:

$$i^k(t) = -\iint_A (\mathcal{E}x_t)^T e_0^k \Lambda^k\, dA \tag{6}$$

$$V^k(t) = -\frac{1}{C^k}\iint_A (\mathcal{E}x)^T e_0^k \Lambda^k\, dA \tag{7}$$

where the film capacitance is defined as

$$C^k \triangleq \iint_A \frac{\varepsilon_0^k}{h^k} \Lambda^k\, dA$$

.

III.   SMTs

In this section, the general theory and design methodology presented in Ref. 8 are reviewed. The SMT theory allows the designer to selectively excite and measure each and every mode of a general anisotropic piezolaminated plate typified in Fig. 1 according to a prespecified set of modal participation factors. Consider the following set of SMT construct conditions.

C1: Exactly n transducer layers are located strictly above the reference plane, and exactly n transducers are located strictly below the reference plane ($N = 2n$).

C2: There are at least six piezoelectrically active layers.

C3: For each layer above the reference plane there exists a layer below the reference plane such that $\{z^k = -z^{k+n}\}_{k=1}^n$.

C4: Layers located at heights z^k and z^{k+n} both are associated with an identical piezoproperty vector $e_\star^k$.

C5: The piezoproperty vectors $\{e_\star^k\}_{k=1}^n$ associated with at least three layers above (and hence also below) the reference plane are different. When the same piezostock material is used throughout, $e_{31}^0(\theta^k = 0\ \text{deg}) \neq e_{32}^0(\theta^k = 0\ \text{deg})$, and the skew angles of at least three laminae above (and hence below) the plane must be different in the range $-90 \leq \theta^k < 90$ deg.

The following lemma was proven in Ref. 8.

Lemma 1: Let $R \in \mathfrak{R}^{6,6}$ be the matrix defined as

$$R \triangleq \sum_{k=1}^{N} e_0^k (e_0^k)^T$$

Then, if conditions C1–C5 hold, R is invertible. Furthermore, R can be written as

$$R = 2\sum_{k=1}^{n}\begin{bmatrix} e_\star^k(e_\star^k)^T & 0 \\ 0 & (z^k)^2 e_\star^k(e_\star^k)^T \end{bmatrix} \tag{8}$$

Let $\bar{\phi}$ be defined as a weighted sum of mode shapes such that

$$\bar{\phi} \triangleq \sum_{j=1}^{\infty} \alpha_j \phi_j, \qquad \alpha_j \in \mathfrak{R} \tag{9}$$

where α_j and ϕ_j are, respectively, the MPF and mode shape corresponding to the jth mode. Allowing each layer to function as a self-sensing actuator,[9,10] the authors proved the following central theorem in Ref. 8.

Theorem 1: Consider an anisotropic rectangular plate containing N piezolaminae whose equations of motion are given by Eq. (1). Assume each piezolamina functions as a self-sensing actuator. Let

the time bound control input $V^k(t)$ of each piezolamina be proportional to an identical time-dependent control function $V_a(t)$ such that $V^k(t) = g_0^k V_a(t)$. Let the measured state $i_s(t)$ formed from the weighted sum of the sensed currents of each individual lamina be such that

$$i_s(t) = \sum_{k=1}^{N} g_0^k i^k(t)$$

Assume that conditions C1–C5 are satisfied. Then, if the piezoelectric field distribution functions of each active layer are given by

$$\Lambda^k = (1/g_0^k)(e_0^k)^T R^{-1} K_a \mathcal{E}\bar{\phi}(x, y) \qquad (10)$$

where $\bar{\phi}$ is defined in Eq. (9), R is defined in Eq. (8), and g_0 is defined as

$$g_0^k = \max_{(x,y) \in A} \left| (e_0^k)^T R^{-1} K_a \mathcal{E}\bar{\phi}(x, y) \right| \qquad (11)$$

the equations of motion of the plate reduce to the form

$$\ddot{q}_m + (b_0 + c_0\lambda)\dot{q}_m + \lambda_m q_m = -\alpha_m \lambda_n V_a(t) \qquad (12)$$

whereas the measured state reduces to the form

$$i_s(t) = -\rho h \sum_{j=1}^{\infty} \alpha_j \lambda_j \dot{q}_j(t) \qquad (13)$$

for all integers $m > 0$, where α_m, λ_m, and $q_m(t)$ are, respectively, the modal participation factor, eigenvalue, and generalized modal coordinate associated with the mth mode.

Should voltage rather than current be preferred as the measured state so that Eq. (7) replaces Eq. (6), then

$$V_s(t) = -\rho h \sum_{j=1}^{\infty} \alpha_j \lambda_j q_j(t) \qquad (14)$$

should replace Eq. (13) (Ref. 11).

Theorem 1 represents an anisotropic piezolaminated plate selective modal actuator and/or sensor design methodology. The SMT construct conditions C1–C5 are obeyed. Mode shapes belonging to the target modal subset are determined and then assigned modal participation factors. Then, using Eq. (10) as an algorithm for determining the piezoelectric field function for each layer and enforcing the condition $V^k(t) = g_0^k V_a(t)$, a modal actuator design is realized that is capable of exciting each mode according to its relative weighting. If instead the condition

$$i_s(t) = \sum_{k=1}^{N} g_0^k i^k(t)$$

is enforced, then a selectively weighted modal measurement may be obtained.

If the composite system is orthotropic so that there is no inherent mechanical coupling between bending and stretching motions, then the differential operators $\mathcal{D}$ and $\mathcal{E}$ simplify[8]:

$$R \stackrel{\Delta}{=} \sum_{k=1}^{N} e_\star^k (e_\star^k)^T$$

replaces its previous definition in Lemma 1, and the following two relaxed conditions replace the SMT construct conditions C1–C5 (Ref. 8).

C6: There are at least three piezoelectrically active layers ($N \geq 3$).

C7: The piezoproperty vectors $\{e_\star^k\}_{k=1}^{N}$ associated with at least three layers are different. When the same piezostock material is used throughout, $e_{31}^0(\theta^k = 0 \deg) \neq e_{32}^0(\theta^k = 0 \deg)$, and the skew angles of at least three laminae must be different in the range $-90 \leq \theta^k < 90$ deg.

IV. Nonselective Modal Transducers (NSMTs)

It is often preferable to develop transducers in which the PFF $\Lambda^k(x, y)$ of each layer is chosen on the basis of facilitating practical implementation rather than selectively assigning modal participation factors to each structural mode. Hence the transducers that result are referred to as NSMTs. However, by expanding the scope of Theorem 1, the set of modal participation factors that correspond to any given NSMT may be predetermined and thus its performance evaluated in the course of synthesizing an appropriate design. The following theorem formalizes the NSMT concept.

Theorem 2: Consider an anisotropic (Kirchhoff–Love) thin plate containing N piezolaminae whose equations of motion are given by Eq. (1). Assume that each lamina is to function as a self-sensing actuator such that the sensed measurement of the kth layer is given by Eq. (13). Assume that conditions C1–C5 are satisfied. Assume also that piezolaminae gain constants $\{g_0^k\}_{k=1}^{N}$ and field functions $\{\Lambda^k\}_{k=1}^{N}$ are known. Let the measured state $i_s(t)$ formed from the weighted sum of the sensed currents of each individual lamina be such that

$$i_s(t) = \sum_{k=1}^{N} g_0^k i_s^k(t)$$

Let the time bound control input $V^k(t)$ of each piezolamina be proportional to an identical time-dependent control function $V_a(t)$ such that $V^k(t) = g_0^k V_a(t)$. Then the equations of motion and measured state are, respectively, reduced to Eqs. (12) and (13) for all integers $j > 0$, where the modal participation factors α_j are given by

$$\alpha_j = \frac{1}{\rho h \lambda_j} \left\langle \mathcal{E}\phi_j, \sum_{k=1}^{N} g_0^k e_0^k \Lambda^k \right\rangle \qquad (15)$$

Remark: As with Theorem 1, conditions C6 and C7 replace conditions C1–C5 when Theorem 2 is applied to orthotropic systems.

Proof: Theorems 1 and 2 both require that conditions C1–C5 are satisfied. Moreover, in both theorems the actuator and sensor equations are, respectively, given by Eqs. (12) and (13). In Theorem 1, however, each PFF (Λ^k) is determined as a function of known MPFs, whereas in Theorem 2 the MPFs are determined from known PFFs. Consequently, Theorem 2 may be proven directly from Theorem 1 through determining which set of MPFs yields a specific set of PFFs. Premultiplying the left side of Eq. (10) by $g_0^k e_0^k$, summing over N layers, applying Lemma 1, and recalling that

$$\bar{\phi} \stackrel{\Delta}{=} \sum_{j=1}^{\infty} \alpha_j \phi_j$$

yields

$$\sum_{k=1}^{N} g_0^k e_0^k \Lambda^k = \sum_{j=1}^{\infty} \alpha_j K_a \mathcal{E}\phi_j \qquad (16)$$

Relying on the identity $\langle \mathcal{E}\phi_i, K_a \mathcal{E}\phi_j \rangle = \rho h \lambda_j \delta_{ij}$ established in Ref. 11,

$$\left\langle \mathcal{E}\phi_m, \sum_{k=1}^{N} g_0^k e_0^k \Lambda^k \right\rangle = \rho h \alpha_m \lambda_m \delta_{jm} \qquad (17)$$

from which Eq. (15) follows trivially. ☐

V. Experimental Validation

The SMT theory was validated through experimental test on a cantilevered orthotropic composite piezolaminated plate. However, resources were not available for selectively doping piezo-copolymer film with a secondary material so as to realize the required PFFs. Instead, commercially available uniformly piezoelectric PVDF was obtained and a single nonselective modal actuator (NSMA) and nonselective modal sensor (NSMS) were designed and then incorporated into the structure. Using Theorem 2, theoretical predictions for the MPFs corresponding to the NSMTs were determined. The resultant NSMTs then become synonymous with SMTs whose MPFs are those that were predicted. Emulating rate feedback of the NSMS measured voltage [Eq. (14)] output through a lead compensation

Table 2 Experimental structure material and geometric properties

Property	PVDF			Graphite-epoxy	
	Layers 1, 10	Layers 2, 9	Layers 3, 8	Layers 4, 7	Layers 5, 6
E_{11}, GPa	2.00	2.00	2.00	14.5	14.5
E_{22}, GPa	2.00	2.00	2.00	9.60	9.60
G_{12}, GPa	1.42	1.42	1.42	4.10	4.10
ν_{12}	0.3	0.3	0.3	0.3	0.3
ρ, kg/m^3	1,780	1,780	1,780	1,551	1,551
Thickness, μm	52	52	104	137.5	137.5
$(e_{31}^0)_{\theta = 0 \text{ deg}}$, C/m^2	60,000	60,000	60,000	——	——
$(e_{32}^0)_{\theta = 0 \text{ deg}}$, C/m^2	20,000	20,000	20,000	——	——
Skew angle θ^k, deg	60	0	-60	22.5	0
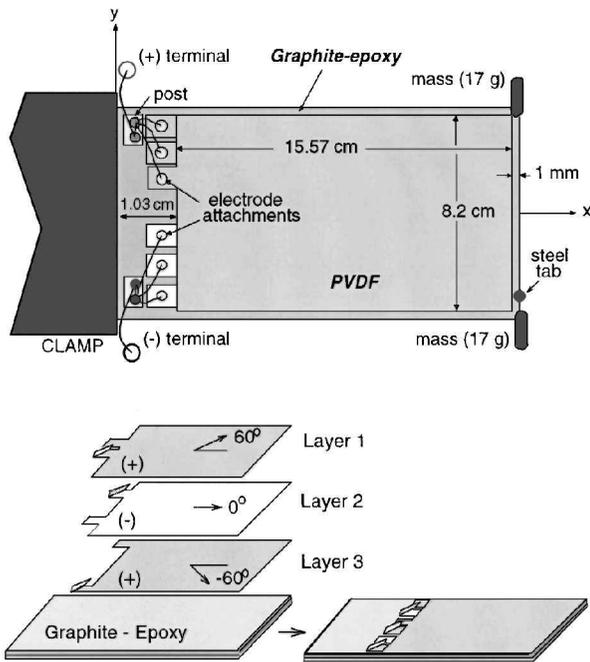
Fig. 2 Test structure, side and exploded views.

Fig. 3 Schematic of test bed configuration (top view).

network, the structure was actively controlled and the closed-loop damping coefficients of the first four vibrational modes were obtained. The rate feedback law was selected because, when ideally implemented, it inherently guarantees stability robustness regardless of piezospatial variance.[7] Significant active vibration attenuation was observed. A numerical simulation of the system was then derived and compared with the actual system behavior. The theoretical results were seen to match the measured response within an expected range of accuracy, thus substantiating the SMT theory.

A. Test Structure Design

The test structure design is illustrated through the side and exploded views given in Fig. 2. The aspect ratio of the plate, whose dimensions are given in Fig. 2, is approximately two. The horizontal and vertical coordinates, respectively, are referred to as x and y. Three PVDF layers were laminated to each face of a 4-layered graphite-epoxy substrate, forming a 10-layered specimen. Skew angle geometry, thickness, and material properties are given in Table 2. Layers are numbered sequentially in the table: layers 1 and 10 are surface laminae. The symmetric layup assures an orthotropic structure and causes the orthotropic SMT construct conditions (C6 and C7) to be immediately satisfied. Each NSMT was constructed via the three PVDF layers (the minimum number required for an orthotropic structure per condition C7) attached to each face of the plate. The piezofield functions of each layer were established as uniformly constant [$\Lambda^k(x, y) = 1$, $k = 1, 2, 3, 8, 9, 10$].

Both the NSMA and NSMS were constructed in an identical manner. The gray and white shading in the exploded view (Fig. 2), respectively, indicate the designated positive and negative electrode surfaces relative to each piezolamina. Hence the $(-)$ electrode of
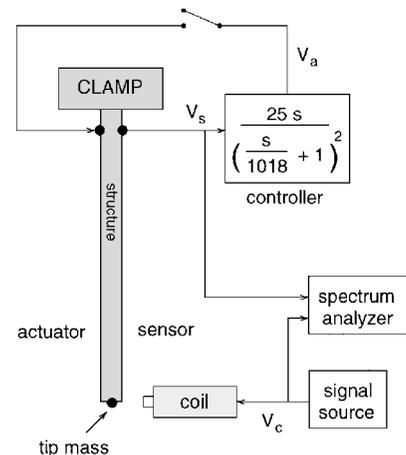
layer 3 rests on the graphite-epoxy substrate, whereas the $(+)$ surfaces of layers 2 and 3 face each other [and similarly the $(-)$ surfaces of layers 1 and 2]. The poling direction of each layer is nonetheless identical; thus when the same voltage command $V_a(t)$ is applied to each layer, $V_1(t) = -V_2(t) = V_3(t) = V_a(t)$. An ordinary low viscosity epoxy was used as the lamination medium. The silver ink electrode coating that normally coats the film surfaces was removed at the film boundaries with methyl ethyl ketone (MEK) so as to avoid electrical arcing in the presence of high voltage fields. Tabs were extended outward from each layer to provide an area for electrode attachments. As shown, electrode attachments to the bottom surfaces of each lamina were facilitated through folding certain tabs in half. The silver ink coating was removed from all positively polarized tab surfaces that rest directly on the substrate because the substrate itself was to be electrically grounded.

Electrode attachments are shown in Fig. 2. Circular attachment points made from thin copper plating were adhered to each lamina tab extension via a silver ink adhesive. Teflon® lead wires from all $(+)$ attach points were then connected at a common post (a strain gauge terminal) on the structure. A secondary wire was then soldered to the post; the possibility of degrading an electrode attachment through tension on a primary wire was thus avoided. The $(-)$ terminal was similarly configured. On the sensor side a nylon sheet was adhered to the exposed outer surface using an extremely thin (5-μm) double-stick tape. The nylon sheet was then covered with a (7-μm) aluminum foil sheet. The foil and the graphite-epoxy substructure were electrically grounded, which effectively eliminated the introduction of radiative noise encountered in other studies.[12] The structure was then cantilevered, and 17 gram masses were attached as close as possible to the free corners both to lower the resonant frequencies of the first few modes and to enhance a torsional response. Lastly, a small steel tab was placed on the structure at the free boundary to allow for the structure to be externally driven by an electromagnet.

B. Experimental Procedure

The test bed configuration is shown schematically in Fig. 3. The structure was driven externally through an electromagnetic coil. The

Table 3 Damping coefficients and natural frequencies: experimental structure

| | Open loop | | Closed loop | | | |
| | | | Theory | | Experiment | |
Mode	ζ_i	ω_i, Hz	ζ_i	ω_i, Hz	ζ_i	ω_i, Hz
1	0.0245	9.2344	0.0657	9.362	0.0710	9.3184
2	0.0342	25.531	0.1135	27.068	0.1157	26.216
3	0.0413	80.370	0.0562	83.751	0.0512	81.463
4	0.0465	127.62	0.0501	128.64	0.0489	129.17

voltage measured across the NSMS terminals, $V_s(t)$, was allowed as an input to a controller block. The controller block was realized through the simple analog circuit cascaded with a high-voltage amplifier. The output of the control block, $V_a(t)$, then drives the NSMA when the switch is closed. Both V_s and the coil drive voltage V_c were processed through a Hewlett-Packard HP5660A spectrum analyzer to acquire the experimental data. The controller, whose transfer function is given in Fig. 3, causes $V_a(t)$ to be nearly proportional to the measured current $i_s(t)$ at low frequencies.

Three experimental test procedures were conducted. In the first procedure, frequency response data relating V_s to the drive coil voltage V_c were obtained in both the open- and closed-loop scenarios. Damping coefficients and resonant frequencies of the first four modes were then determined. A free decay test was then performed: the structure was excited via the drive coil at a modal frequency until a steady-state response was obtained, and then the excitation was removed. Open- and closed-loop time histories were thus obtained for the first three structural modes. Last, the structure was subject to continuous excitation at a resonance frequency with the controller off, and the time history was recorded as the controller was turned on. The latter procedures served to demonstrate controller performance, whereas the frequency response test provided damping coefficient and resonance frequency data necessary to validate the theoretical model.

C. Experimental Results
Frequency Response

The magnitude of the transfer function V_s/V_c obtained for the first four modes is given in Fig. 4 (phase plots may be found in Ref. 11). The solid lines indicate the uncontrolled response, whereas the dashed lines represent the controlled response. To obtain a high level of coherence, the system was repeatedly driven through a 0.02-Hz/s sinusoidal sweep in the vicinity of each mode. Mode shapes, as determined by the numerical analysis to follow, are described in Sec. V.D. Open- and closed-loop natural frequency and damping coefficients are given in Table 3. Damping coefficients were obtained using the half-power bandwidth method.[11]

Free Decay Test

Free decay test results for the first three modes are given in Figs. 5–7. The instant in which the sinusoidal excitation to the drive coil is turned off is indicated in each time history by a vertical dashed line. In all cases, significant active vibration suppression is observed. In the second mode response (Fig. 6), removal of the input tended to marginally excite first mode oscillations as well. The high-frequency ripple in the second and third mode controlled responses is attributed to 50-Hz line noise that entered the system through the control electronics.

Continuous Excitation Test

First, second, and third mode continuous excitation test results are shown in Fig. 8. The introduction of active control is indicated by the vertical dashed line in both time histories. A significant reduction in the amplitude of the vibrational response of all three modes is observed when the controller is turned on.

D. Theoretical Results

Applying Theorem 2, the authors determined the MPFs corresponding to the transducers implemented on the experimental structure. The NSMT themselves may then be thought of as SMTs whose
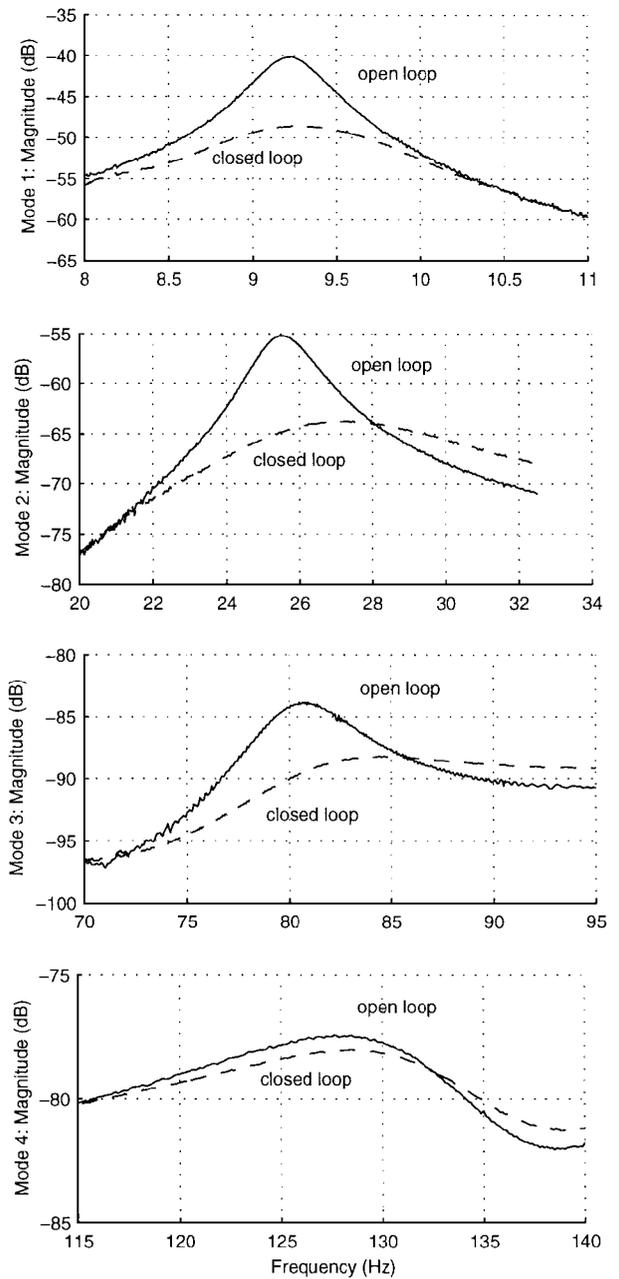
Fig. 4 Frequency response data: ——, uncontrolled system and – – –, actively controlled system.

MPFs are those determined via Theorem 2. The experimental structure satisfies both orthotropic plate construct conditions C6 and C7. For orthotropic plates in bending, Eq. (15) is reduced to the form

$$\alpha_j = \frac{1}{\rho h \lambda_j} \left\langle \mathcal{E}_b \phi_j^b, \sum_{k=1}^{N} g_0^k z^k \mathbf{e}_\star^k \Lambda^k \right\rangle \tag{18}$$

where

$$\mathcal{E}_b = -\left[\frac{\partial^2}{\partial x^2} \quad \frac{\partial^2}{\partial y^2} \quad 2\frac{\partial^2}{\partial x \partial y}\right]^T \tag{19}$$

based on simplifications found in Ref. 8. The jth out-of-plane bending mode is referred to as $\phi_j^b[w(x, y)]$. In the experimental structure all $\Lambda^k = 1$, whereas the electrical attachments and layer polarities ensure that $(g_0^1, g_0^2, g_0^3) = (g_0^8, g_0^9, g_0^{10}) = (1, -1, 1)$. Hence the MPFs identified with the experimental structure may be readily calculated once mode shapes are determined.

A discrete model of the experimental structure was developed to obtain high-fidelity mode shape approximations. The ANSYS finite element modeling (FEM) package[13] was used to generate mass and stiffness matrices ($\mathbf{M}$ and $\mathbf{K}$). The eigenfunctions obtained through
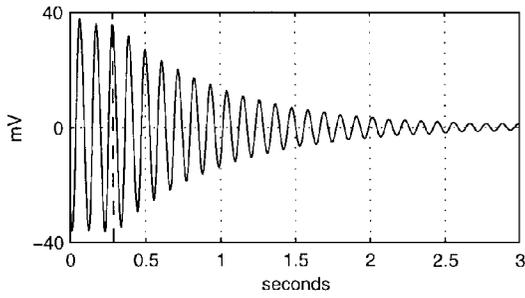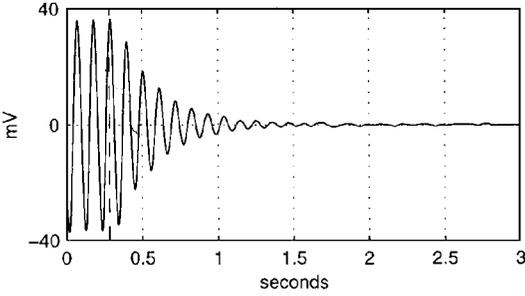
Fig. 5   First mode free decay test results.
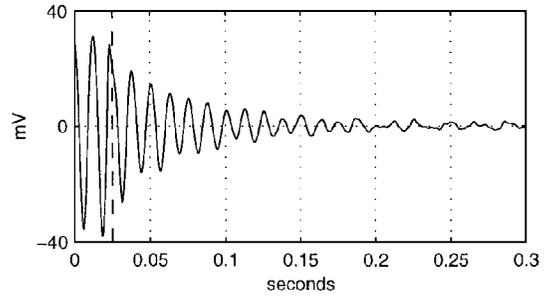
Fig. 6   Second mode free decay test results.
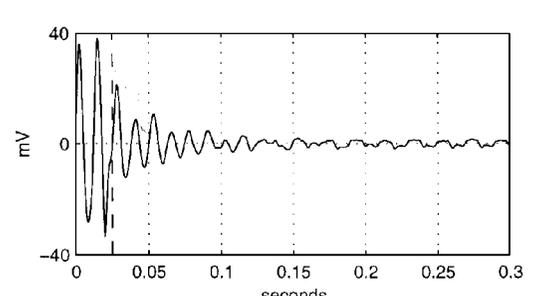
Fig. 7   Third mode free decay test results.
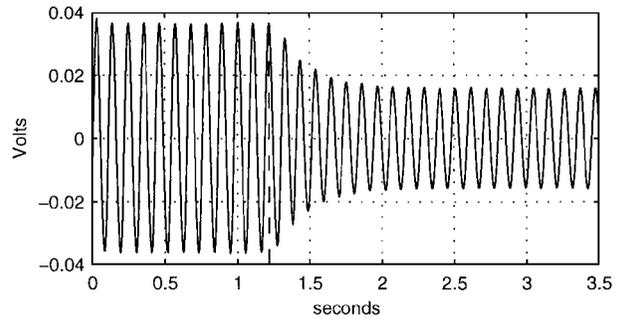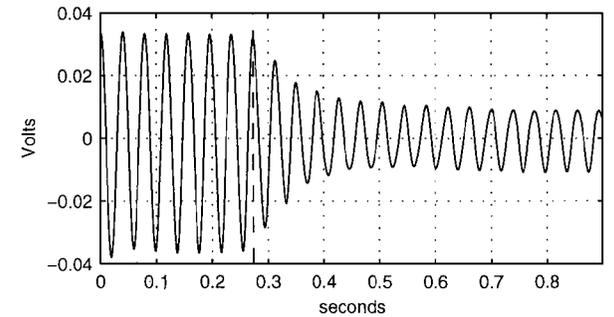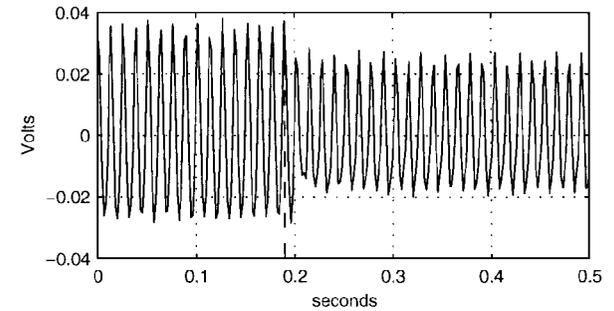
Fig. 8   Continuous excitation test results. Vertical dashed lines indicate moment at which controller is turned off.

the FEM analysis, the first four of which are shown in Fig. 9, were then best fit (in a least-squares sense) to a polynominal of the form

$$\phi_j^b = [x^6 \quad x^5 \quad x^4 \quad x^3 \quad x^2 \quad x \quad 1]$$
$$\cdot P[y^6 \quad y^5 \quad y^4 \quad y^3 \quad y^2 \quad y \quad 1]^T \tag{20}$$

where $P \in \Re^{7,7}$ is a polynomial coefficient matrix. Boundary constraints were included in the determination of P to improve the fidelity of the approximation (see Sec. V.E). Equation (20) was then used in conjunction with Eq. (18) to determine the MPFs corresponding to the first 10 structural modes. Errors associated with FEM open-loop eigenvalue predictions were essentially eliminated through setting the first four open-loop natural frequencies and damping factors to experimentally observed values.

To theoretically predict the closed-loop damping coefficients and natural frequencies, the (open-loop) system was represented in the modally decomposed form

$$\ddot{q} + \bar{C}\dot{q} + \bar{K}q = f_q V_a(t) \tag{21}$$
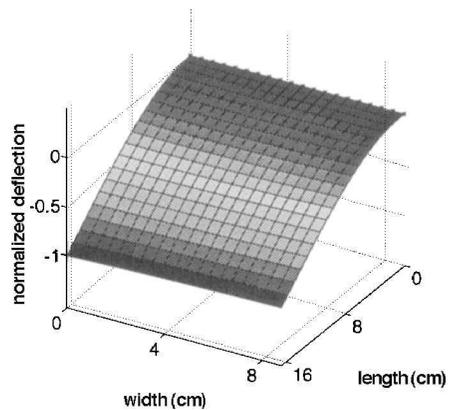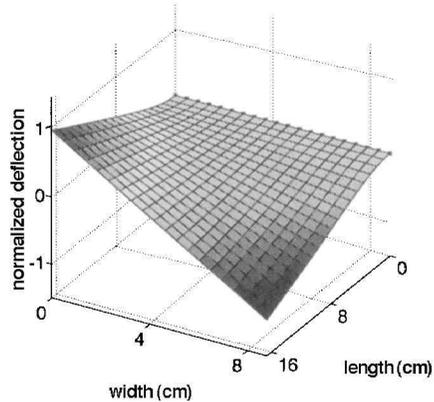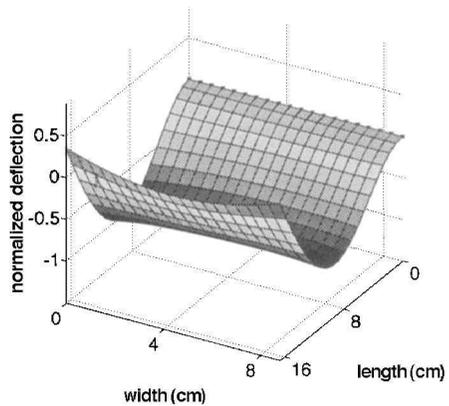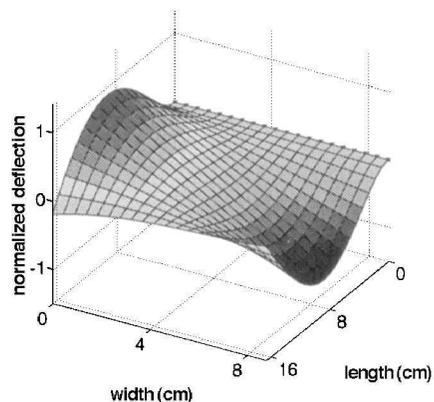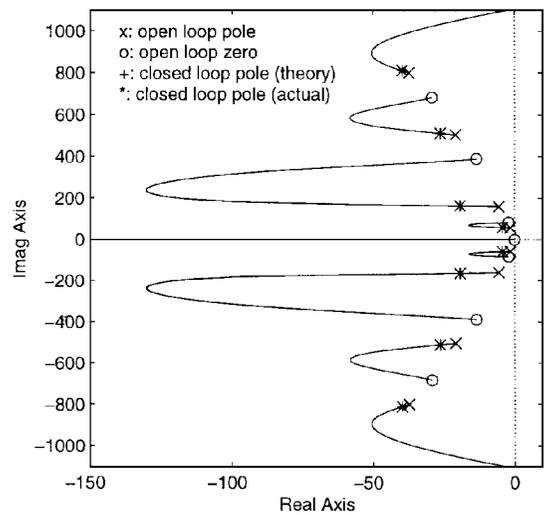
Fig. 10 Root locus of experimental structure. Because predicted closed-loop pole locations closely match measured values, theoretical and actual closed-loop eigenvalue locations are indistinguishable in this plot.

where the modal vector $q \in \mathfrak{R}^{10}$ and modal stiffness matrix $\bar{K} \in \mathfrak{R}^{10,10}$ were determined through an ordinary modal decomposition performed on the discrete FEM. Equation (21) is merely a discretization of Eq. (12). The modal force vector is defined as $f_q = [\alpha_1 \lambda_1, \ldots, \alpha_{10} \lambda_{10}]$, where $\lambda_j = (\omega_j)^2$ is formed from experimentally observed open-loop natural frequency values. Actual experimentally obtained open-loop damping coefficients were likewise used to form $\bar{C}$. The disturbance force introduced into the system via the drive coil was not included in the model because its inclusion has no bearing on the closed-loop damping coefficients and natural frequencies. Because the measured voltage $V_s(t)$ is related to the current flow through the sensor i_s, such that

$$i_s = C_s \frac{dV_s}{dt} \tag{22}$$

where C_s is the NSMS capacitance, then upon discretization of the output equation in Theorem 2, the NSMS measurement is approximated as

$$V_s = -(1/C_s) f_q^T q \tag{23}$$

where the minus sign accommodates the reverse polarity of NSMS transducers relative to the NSMA transducers. The capacitance C_s was measured and found to be 108 nF. In first-order form the open-loop system equations become

$$\frac{d}{dt} \begin{bmatrix} q \\ \dot{q} \end{bmatrix} = \begin{bmatrix} 0 & 1 \\ -\bar{K} & -\bar{C} \end{bmatrix} \begin{bmatrix} q \\ \dot{q} \end{bmatrix} + \begin{bmatrix} 0 \\ f_q \end{bmatrix} V_a \tag{24}$$

$$V_s = \begin{bmatrix} -(1/C_s) f_q^T & 0 \end{bmatrix} \begin{bmatrix} q \\ \dot{q} \end{bmatrix} \tag{25}$$

The controller was similarly expressed in the first-order form

$$\dot{x}_c = A_c x_c + B_c V_s \tag{26}$$

$$V_a = C_c x_c \tag{27}$$

where the definitions are obvious. Closed-loop system poles were then found by combining the four preceding equations to form a closed-loop system. Damping factors and natural frequencies corresponding to the (predicted) closed-loop poles are tabulated in Table 3. By introducing a multiplicative factor k into the controller output equation such that $V_a = k C_c x_c$, the root locus of the predicted closed-loop pole locations as a function of k was determined and is given in Fig. 10. Predicted pole locations ($k = 1$) are indicated by a ($+$) sign, and experimental pole locations are designated with an asterisk ($*$). The system is unstable for high feedback gains: the predicted gain margin of the experimental controller was found to be 30.447 (29.671 dB).

Mode 1

Mode 2

Mode 3

Mode 4

Fig. 9 First four mode shapes of experimental structure as generated by ANSYS FEM code.

E. Analysis of Results

As shown in Table 3, the predicted damping coefficient values are close to the experimentally obtained values. The fidelity of the closed-loop eigenvalue predictions renders as indistinguishable the theoretical and measured closed-loop pole locations in Fig. 10. A quantitative comparison between predicted and measured damped natural frequency values yields a worst case 3.28% error for mode 2. Modes 1 and 4 yield error margins less than 0.5%. Several error sources exist, which are likely to account for the discrepancies between the predicted and actual behavior of the experimental system, and are now briefly discussed.

Finite Element Model

FEM mode shape predictions enter directly into the theoretical model via Eq. (18) and hence directly affect the accuracy of the theortical solution. FEM predicted open-loop natural frequencies of the first four modes are known to deviate as much as 8% from actual measured values.[11] FEM mode shape predictions, and thus MPF predictions, are then reasonably assumed to be similarly accurate to within 8% of actual values.

Numerical Errors

To solve Eq. (18), actual mode shape data obtained through the FEM were fit to a polynomial of the form given in Eq. (20) through a (nonweighted) least-squares minimization. Although the polynomic functions were constrained to satisfy all geometric boundary conditions, natural boundary conditions were not necessarily satisfied. Hence the polynomic mode shape approximations are expected to lack some fidelity in predicting the true MPF values associated with the experimental structure, although the resulting margin of error is difficult to quantify.

Data Measurement

The accuracy of measured data is dependent on the fidelity of the discrete data sampling and signal processing methods employed as well as the quality of isolation of the test bed environment. Air currents, floor vibrations, and electromagnetic radiation were seen to induce measurable signals. Although great care was taken to minimize extraneous noise sources and to enhance accurate data collection, some error is inevitably introduced.

In consideration of all of the aforementioned error sources, error margins as large as 10% could have been reasonably assumed. Hence the fidelity of the preceding results falls well within the expected margins and serves to validate the SMT concept as applied to an orthtropic plate.

F. Design Considerations

The final experimental structure design was the outcome of a lengthy evolutionary process. Several findings of that process are now discussed.

Air Gaps

Extreme care must be taken to ensure that no significant air gaps exist between active surfaces, as voltage transients may otherwise develop that will generate enough heat to destroy the integrity of the film. In this regard, the weakest part of any design attempted was found to be the attachment of the lead wire to the surface of the PVDF film. The attachment was made by soldering the lead wire to a thin copper tab and then bonding the tab to the film surface via a silver ink paste. Care must be taken to remove any air gaps that may exist underneath the lead attachment. In an earlier design each layer was folded in half, and lead attachments were buried in the structure in accord with an isotropic beam experimental design used by Lee et al.[14] Folding each layer in half and grounding the outer surface provide good shielding against electromagnetic noise, which otherwise would be detected by the sensors. However, burying the lead attachments created air gaps that destroyed film layer integrity. In the present design, lead attachments were exposed so that failed attachments could be easily repaired.

In the present design, the film attachment regions were folded in half to attach lead wires to those film surfaces facing toward the substrate. To insulate the positive surfaces from the electrically grounded substrate, thin pieces of Mylar® were placed underneath the film tabs, which inadvertently created an air gap between the PVDF film and the substrate. Consequently, during the test, a high-voltage transient developed and destroyed the integrity of the film in a local region near the lead attachment point to layer 2. In future experiments it would be advisable to place a Mylar sheet (or other insulatory material) along the entire surface between the substrate and adjoining film layers.

Film Boundaries

Voltage arcing commonly occurs across film edges if care is not taken to remove the (manufacturer-deposited) silver ink electrode coating on the film surfaces near all boundaries. MEK is an excellent solvent for this purpose.

Radiative Noise

The PVDF film layers are highly sensitive to sources of electromagnetic noise. Care should be taken to properly shield the film surfaces. The current design was seen to perform fairly well in this respect.

Lamination

The bonds between laminae must be both thin and uniform (in particular, free of air bubbles). An ordinary slow dry (24-h) epoxy worked very well in this regard. Heat should be applied when mixing the epoxy and hardening agent. The bleeding process (squeezing out excess epoxy) is critical to ensure thin interlaminar regions: weight should be applied evenly to the surface during cure. In the current design, a stress of 0.6 kg/cm^2 was applied during the dry. Although the bleeding process was excellent in the current design (interlaminar thicknesses on the order of 2–3 μm), the previous Lee et al.[14]-type folded-layer design was deficient in this respect. In that design, epoxy could not flow freely along the folded edge, and hence interlaminar thicknesses exceeded 20 μm. It was also observed that the epoxy-filled interlaminar regions never were seen to provide any electrical insulation between adjoining layers.

In designing the NSMS, an extremely thin (< 5 μm) double-sided tape was tried as an interlaminar adhesive and was seen to perform well. The tape also provided electrical insulation between layers. Bonding appeared to be excellent. Nonetheless, this approach cannot be used for high voltage applications and is assumedly inappropriate when specimen longevity is a primary factor.

VI. Conclusions

A general SMT design methodology recently introduced by the authors for piezolaminated anisotropic plate systems was reviewed and then extended to provide the means to predict the modal character of multilayered piezolaminated transducers embedded in an anisotropic plate. The SMT theory was then validated through experimental test. An experimental procedure was described involving a 10-layered orthotropic plate constructed from 4 graphite-epoxy layers sandwiched between 6 piezoelectrically active PVDF sublaminae. Three PVDF sublaminae stacked on each face were combined electrically to provide both a sensed measurement and an actuation channel with predicted modal content. Lead compensation was employed to provide active control. Open- and closed-loop frequency and transient response data were collected, and significant active vibration attenuation was observed. A numerical simulation directly based on an SMT-derived transducer model was developed and then compared with the actual system behavior. The theoretically based numerical results were seen to closely resemble the measured response and to fall within expected error bounds. Several implementation issues were identified and discussed.

References

[1]Bailey, T., and Hubbard, J., "Distributed Piezoelectric Polymer Active Vibration Control of a Cantilever Beam," *Journal of Guidance, Control, and Dynamics*, Vol. 8, No. 5, 1985, pp. 605–611.

[2]Burke, S., and Hubbard, J. E., "Distributed Actuator Control Design for Flexible Beams," *Automatica*, Vol. 24, No. 5, 1988, pp. 619–627.

[3]Miller, S. E., and Hubbard, J. E., "Smart Components for Structural Vibration Control," *Proceedings of the 1988 Automatic Controls Conference*, Vol. 3, Inst. of Electrical and Electronics Engineers, New York, 1988, pp. 1897–1902.

[4]Burke, S. E., and Hubbard, J. E., "Distributed Transducer Control Design for Thin Plates," *Conference on Electro-Optical Materials for Switches, Coatings, Sensor Optics, and Detectors*, Vol. 1307, Society of Photo-Optical Instrumentation Engineers, Orlando, FL, 1990, pp. 222–231.

[5]Lee, C. K., "Theory of Laminated Piezoelectric Plates for the Design of Distributed Sensors and Actuators. Part1: Governing Equations and Reciprocal Relationships," *Journal of the Acoustical Society of America*, Vol. 87, No. 3, 1990, pp. 1144–1158.

[6]Miller, S., Abramovich, H., and Oshman, Y., "Active Distributed Vibration Control of Anisotropic Piezoelectric Laminated Plates," *Journal of Sound and Vibration*, Vol. 183, No. 5, 1995, pp. 797–817.

[7]Miller, S., Oshman, Y., and Abramovich, H., "Modal Control of Piezolaminated Anisotropic Rectangular Plates: Part 1—Modal Transducer Theory," *AIAA Journal*, Vol. 34, No. 9, 1996, pp. 1868–1875.

[8]Miller, S., Oshman, Y., and Abramovich, H., "Modal Control of Piezolaminated Anisotropic Rectangular Plates: Part 2—Control Theory," *AIAA Journal*, Vol. 34, No. 9, 1996, pp. 1876–1885.

[9]Anderson, E. H., Hagood, N. W., and Goodcliffe, J. M., "Self-Sensing Piezoelectric Actuation: Analysis and Application to Controlled Structures," *Proceedings of the AIAA/ASME/ASCE/AHS/ASC 33rd Structures, Structural Dynamics, and Materials Conference* (Dallas, TX), AIAA, Washington, DC, 1992, pp. 2141–2155 (AIAA Paper 92-2465).

[10]Dosch, J., Inman, D., and Garcia, E., "A Self-Sensing Piezoelectric Actuator for Collocated Control," *Journal of Intelligent Materials and Structures*, Vol. 3, Jan. 1992, pp. 166–185.

[11]Miller, S. E., "Distributed Modal Control of Piezolaminated Anisotropic Planar and Cylindrical Structures," Sc.D. Thesis, Faculty of Aerospace Engineering, Technion—Israel Inst. of Technology, Haifa, Israel, Aug. 1995.

[12]Miller, S. E., and Hubbard, J. E., "Observability of a Bernoulli-Euler Beam Using PVF2 as a Distributed Sensor," *Proceedings of the 6th VPI&SU/ AIAA Symposium on Dynamics and Control of Large Structures*, Virginia Polytechnic Inst. and State Univ., Blacksburg, VA, 1987, pp. 375–390.

[13]Swanson Analysis Systems, "ANSYS User's Manual for Revision 5.0," Houston, PA, 1992.

[14]Lee, C. K., Chiang, W. W., and O'Sullivan, T. C., "Piezoelectric Modal Sensor and Actuator Pairs for Critical Active Damping Vibration Control," *Journal of the Acoustical Society of America*, Vol. 90, No. 1, 1991, pp. 374–384.

A. Berman
Associate Editor